KFUPM
Journal of Undergraduate Research International

Diamond Open Access 66

Article Control and Instrumentation Engineering

Proportional-Derivative Self-Learning Control for Robust Quadrotor UAV Trajectory Tracking under Disturbances

Abdulrahman Sulaiman Al-Sayed and Syed Muhammad Amrr*

Cite https://doi.org/10.64589/juri/231618

Submitted: April 22, 2026 **Revised:** May 17, 2026 **Accepted:** July 09, 2026

ABSTRACT

This study presents a proportional derivative-self learning control (PD-SLC) strategy for trajectory tracking of quadrotor unmanned aerial vehicles operating under external disturbances. The proposed method integrates conventional PD control with a memory mechanism that reuses prior control inputs, thereby enhancing adaptability and disturbance rejection while maintaining a simple and implementable structure. Unlike conventional adaptive or robust controllers that require complex parameter estimation, the PD-SLC framework accelerates transient convergence, reduces steady-state control effort, and improves responsiveness in repetitive maneuvers. Closed-loop stability analysis is established through Lyapunov analysis, confirming that all system signals remain bounded and that tracking errors converge within predefined limits despite uncertainties. Numerical simulations under time-varying disturbance scenarios validate the effectiveness of the approach. Results demonstrate that the PD-SLC achieves reductions of up to 44.7% in the integral of squared error and 57.1% in the integral of time-weighted absolute error compared with proportional-integral-derivative control. Additionally, the controller produces smoother control signals and requires lower actuator effort than sliding mode control. Overall, the proposed PD-SLC scheme offers a practical balance between simplicity and robustness, making it suitable for real-world quadrotor applications where efficiency and reliability are critical.

Keywords: attitude control, position control, uniformly ultimately bounded, robust control, Lyapunov analysis, unmanned aerial vehicle

1. INTRODUCTION

In recent years, unmanned aerial vehicles (UAVs) have attracted considerable attention, as both researchers and industry professionals recognize their potential across diverse real-world applications. UAVs are increasingly employed for infrastructure assessment, environmental monitoring, security operations, and parcel delivery. Their growing use in both hazardous and routine tasks underscores the need for reliable protocols that ensure safe and accurate operation. Consequently, the research community has intensified efforts to develop control systems that deliver robust performance. Among UAV configurations, the quadrotor has emerged as a favored option owing to its operational versatility and ease of use. However, quadrotors often struggle to maintain stable flight under environmental disturbances and uncertainties, creating challenges for reliable operation. To address these issues, numerous control approaches have been investigated[1].

Traditional linear control methods, such as proportional-integral-derivative (PID) controllers and linear quadratic regulators, are widely applied to quadrotor systems. These schemes are simple, easy to implement, and provide acceptable performance under stable or slightly varying conditions. However, they become inadequate in the presence of strong disturbances, nonlinear dynamics, or uncertain parameters. Mo and Farid[2] presented a comprehensive review of nonlinear and modern control techniques for quadrotors, highlighting the growing interest in advanced approaches to overcome the limitations of conventional methods.

Nonlinear controllers such as backstepping and sliding mode control (SMC) have been extensively studied for UAV trajectory tracking[3–5]. Backstepping offers a systematic design framework but can be less robust under uncertainties and often results in complex formulations[6]. SMC is well known for its robustness against disturbances and uncertainties. However, its discontinuous switching action induces chattering, a high-frequency oscillation that can damage actuators, increase energy consumption, and degrade performance[7,8].

Adaptive control methods have been explored to reduce reliance on precise system models by adjusting parameters in real time to deal with uncertainties and dynamic changes in the system[9,10]. These methods have also been combined with SMC to adapt control gains, thereby mitigating the chattering problem while maintaining robustness[11,12]. However, adaptive control can increase system complexity by raising the order of the controller, and poor parameter tuning may lead to slow response or even instability. Additionally, adaptive schemes are sensitive to measurement noise, which can introduce undesirable transient effects. Although adaptive control enhances flexibility and robustness, its practical application to real-world systems remains

Published under an exclusive license by KFUPM

challenging owing to implementation complexity and sensitivity to external disturbances [9,11].

Recently, self-learning control (SLC) has gained attention as a simple and efficient approach for dynamic systems. In this method, the present control input is merged with a weighted version of the past input, providing the system with memory that progressively enhances performance [13,14]. This straightforward design eliminates the need for intricate adaptation rules, parameter estimation, or observer-based strategies typically required in advanced control techniques. Consequently, SLC improves resilience to disturbances and uncertainties, enhances transient behavior, and achieves superior tracking performance without introducing significant complexity [15].

SLC was first introduced for spacecraft attitude control [13,16]. Its control law incorporates a learning term based on prior inputs together with an updating term to enable the system to utilize past control information. Stability under disturbances is maintained through an algebraic formulation that is simple to implement. Although the method initially requires higher energy owing to the learning process, it becomes more energy-efficient over time compared with conventional approaches. Subsequent research [14] extended the original fixed-gain design by introducing a variable-learning approach to address its limitations. By reducing the influence of the learning term during steady operation, the method improves actuator performance while maintaining accurate trajectory tracking. This refinement preserves the benefits of self-learning while mitigating excessive control effort. The approach was later applied to multi-agent systems [15], where it was tested on models with linear dynamics and bounded disturbances. Lyapunov-based analysis confirmed closed-loop stability and demonstrated that tracking errors remained within predefined bounds, further validating the robustness and applicability of the method.

Although SLC shows considerable potential, its application to UAV systems remains limited. Further research is needed to evaluate its performance, particularly in terms of stability and robustness, and to develop control strategies that are both effective and practical for real-world UAV operations. Motivated by this gap, the present study investigates the use of SLC for quadrotor trajectory tracking under external disturbances. The main contributions of this work are summarized as follows:

- Proportional-derivative (PD)-based SLC (PD-SLC) strategy: A novel PD-SLC framework is proposed for quadrotor UAVs operating under external disturbances and model uncertainties. Unlike conventional adaptive or robust controllers, which often require complex parameter estimation and high computational resources, the proposed method leverages prior control input information to improve adaptability and disturbance rejection while maintaining a simple and implementable structure. This design choice enhances practicality for real-time UAV applications, where computational efficiency and ease of implementation are critical.
- Enhanced trajectory tracking: The framework is specifically designed to improve the trajectory tracking performance of quadrotor systems in the presence of nonlinear dynamics, aerodynamic effects, and environmental disturbances such as wind gusts. By integrating proportional and derivative learning terms into the SLC structure, the controller achieves smoother transient responses, faster convergence of tracking errors, and enhanced robustness against uncertainties. The use of historical control information enables the system to learn from past responses, thereby improving tracking accuracy over repeated operations without significantly increasing complexity.
- Rigorous stability analysis: A Lyapunov-based stability analysis is developed to mathematically validate the effectiveness of the proposed control scheme. The analysis demonstrates that all closed-loop system signals remain bounded, and that tracking errors asymptotically converge within predefined limits despite the presence of disturbances and uncertainties.
- Comparative evaluation: Extensive numerical simulations are conducted under various operating scenarios and disturbance conditions. The proposed controller is benchmarked against SMC and conventional PID control. The results confirm that the proposed PD-SLC method achieves superior trajectory tracking performance, reduced steady-state error, faster response and settling times, and lower control effort compared with the reference methods.

The remainder of this paper is organized as follows. Section 2 introduces the quadrotor model along with some essential preliminaries. Section 3 presents the construction of the proposed PD-SLC and its stability analysis. Section 4 discusses simulation results and comparative evaluation. Finally, Section 5 provides the conclusions.

2. PROBLEM FORMULATION

A quadrotor UAV is a six-degree-of-freedom system comprising three translational and three rotational motions about the coordinate axes. By varying the rotor speed, the vehicle can generate thrust and torque to maneuver in any direction. The quadrotor's position in three-dimensional (3D) space is represented by the coordinates (z, x, y), while its orientation is described by the Euler angles $(\varphi, \vartheta, \Psi)$, which correspond to roll, pitch, and yaw, respectively. The overall dynamics can be divided into two coupled subsystems: (i) attitude dynamics, which govern rotational motion, and (ii) position dynamics, which control translational motion.

Attitude subsystem: The mathematical model of the attitude subsystem is expressed as [17]

$$\begin{cases} \ddot{\varphi} = \dot{\vartheta}\dot{\Psi}a_x + U_2 b_x + d_\varphi \\ \ddot{\vartheta} = \dot{\varphi}\dot{\Psi}a_y + U_3 b_y + d_\vartheta \\ \ddot{\Psi} = \dot{\varphi}\dot{\vartheta}a_z + U_4 b_z + d_\Psi \end{cases} \tag{1}$$

where coefficients a_i and b_i for $i \in \{x, y, z\}$ are defined as

$$a_x = \frac{\mathcal{J}_y - \mathcal{J}_z}{\mathcal{J}_x}, \quad a_y = \frac{\mathcal{J}_z - \mathcal{J}_x}{\mathcal{J}_y}, \quad a_z = \frac{\mathcal{J}_x - \mathcal{J}_y}{\mathcal{J}_z},$$
$$b_i = \frac{1}{\mathcal{J}_i}$$

and $\mathcal{J}_x$, $\mathcal{J}_y$, and $\mathcal{J}_z$ are the principal moments of inertia; d_φ, d_ϑ, and d_Ψ denote the external disturbances on each rotational axis; and U_2, U_3, and U_4 are control torques for the respective axis.

Position subsystem: The position dynamics of UAVs are expressed as[17]

$$\begin{cases} \ddot{z} = \dfrac{U_1}{m}\cos(\varphi)\cos(\vartheta) - g + d_z \\ \ddot{x} = \dfrac{U_1}{m}\mathcal{U}_x + d_x \\ \ddot{y} = \dfrac{U_1}{m}\mathcal{U}_y + d_y \end{cases} \tag{2}$$

where U_1 is the total thrust; $\mathcal{U}_x = \cos(\varphi)\sin(\vartheta)\cos(\Psi) + \sin(\varphi)\sin(\Psi)$; $\mathcal{U}_y = \cos(\varphi)\sin(\vartheta)\sin(\Psi) - \sin(\varphi)\cos(\Psi)$; g is the gravitational acceleration; m is the total mass; and d_x, d_y, and d_z are the external disturbances on each translational axis.

Subsystems (1) and (2) can be expressed in a compact vector form with $\mathcal{R} = [\varphi, \vartheta, \Psi]^T \in \mathbb{R}^3$ and $\ddot{\mathcal{R}} = [z, x, y]^T \in \mathbb{R}^3$ as

$$\ddot{\mathcal{R}} = \mathcal{F}_{\mathcal{R}} + \mathcal{G}_{\mathcal{R}}\mathcal{U}_{\mathcal{R}} + \mathcal{D}_{\mathcal{R}} \tag{3}$$

$$\ddot{\mathcal{P}} = \mathcal{F}_{\mathcal{P}} + \mathcal{G}_{\mathcal{P}}\mathcal{U}_{\mathcal{P}} + \mathcal{D}_{\mathcal{P}} \tag{4}$$

where $\mathcal{U}_{\mathcal{R}} = [U_2, U_3, U_4]^T \in \mathbb{R}^3$; $\mathcal{U}_{\mathcal{P}} = [U_1, \mathcal{U}_x, \mathcal{U}_y]^T \in \mathbb{R}^3$; $\mathcal{D}_{\mathcal{R}} = [d_\varphi, d_\vartheta, d_\Psi]^T \in \mathbb{R}^3$; and $\mathcal{D}_{\mathcal{P}} = [d_z, d_x, d_y]^T \in \mathbb{R}^3$. The nonlinear drift terms are $\mathcal{F}_{\mathcal{R}} := [\dot{\vartheta}\dot{\Psi}a_1, \dot{\varphi}\dot{\Psi}a_2, \dot{\varphi}\dot{\vartheta}a_3]^T \in \mathbb{R}^3$ and $\mathcal{F}_{\mathcal{P}} := [-g, 0, 0]^T \in \mathbb{R}^3$, while the input gain matrices are $\mathcal{G}_{\mathcal{R}} = \mathrm{diag}(b_x, b_y, b_z) \in \mathbb{R}^{3\times3}$ and $\mathcal{G}_{\mathcal{P}} = \mathrm{diag}(\cos(\varphi)\cos(\vartheta)/m, 1/m, 1/m) \in \mathbb{R}^{3\times3}$.

2.1. Error Dynamics. The primary objective of the control law $\mathcal{U} = [U_1, U_2, U_3, U_4]^T \in \mathbb{R}^4$ is to accurately track the reference trajectory. The tracking errors are defined as $\mathcal{E}_{\mathcal{R}} = \mathcal{R} - \mathcal{R}_d$ and $\mathcal{E}_{\mathcal{P}} = \mathcal{P} - \mathcal{P}_d$, where $\mathcal{R}_d = [\varphi_d, \vartheta_d, \Psi_d]^T$ and $\mathcal{P}_d = [z_d, x_d, y_d]^T$ are the respective desired trajectories. To facilitate controller design, the following state transformations are introduced:

- Attitude errors: $\boldsymbol{\delta}_{\mathcal{R}1} = \mathcal{E}_{\mathcal{R}}$ and $\boldsymbol{\delta}_{\mathcal{R}2} = \mathcal{E}_{\mathcal{R}}$
- Position errors: $\boldsymbol{\delta}_{\mathcal{P}1} = \mathcal{E}_{\mathcal{P}}$ and $\boldsymbol{\delta}_{\mathcal{P}2} = \mathcal{E}_{\mathcal{P}}$

Using these transformed variables, the error dynamics for attitude and position can be expressed based on Eqs. (3) and (4):

$$\begin{cases} \dot{\boldsymbol{\delta}}_{\mathcal{R}1} = \boldsymbol{\delta}_{\mathcal{R}2} \\ \dot{\boldsymbol{\delta}}_{\mathcal{R}2} = F_{\mathcal{R}} + \mathcal{G}_{\mathcal{R}}\mathcal{U}_{\mathcal{R}} + \mathcal{D}_{\mathcal{R}} - \ddot{\mathcal{R}}_d \end{cases} \tag{5}$$

$$\begin{cases} \dot{\boldsymbol{\delta}}_{\mathcal{P}1} = \boldsymbol{\delta}_{\mathcal{P}2} \\ \dot{\boldsymbol{\delta}}_{\mathcal{P}2} = \mathcal{F}_{\mathcal{P}} + \mathcal{G}_{\mathcal{P}}\mathcal{U}_{\mathcal{P}} + \mathcal{D}_{\mathcal{P}} - \ddot{\mathcal{P}}_d \end{cases} \tag{6}$$

Assumption 1. *The external disturbances $\mathcal{D}_{\mathcal{P}}$ and $\mathcal{D}_{\mathcal{R}}$ are bounded, i.e., $\| \mathcal{D}_{\mathcal{P}} \| \leq \bar{d}_{\mathcal{P}}$ and $\| \mathcal{D}_{\mathcal{R}} \| \leq \bar{d}_{\mathcal{R}}$, where $\bar{d}_{\mathcal{P}}$ and $\bar{d}_{\mathcal{R}} > 0$ are known constants.*

2.2. Problem Statement. The objective of this study is to design an SLC law $\mathcal{U}(t)$ for a quadrotor to track its time-varying trajectory under external disturbances. Specifically, the controller should achieve

$$\lim_{t\to\infty} \| \boldsymbol{\delta}_{\mathcal{R}1}(t) \| \leq b_{\mathcal{R}} \quad \text{and} \quad \lim_{t\to\infty} \| \boldsymbol{\delta}_{\mathcal{P}1}(t) \| \leq b_{\mathcal{P}} \tag{7}$$

where $b_{\mathcal{P}} > 0$ and $b_{\mathcal{R}} > 0$ are small residual bounds whose sizes are characterized in Theorem 1. In the disturbance-free case, i.e., when $\mathcal{D}_{\mathcal{P}} = \mathcal{D}_{\mathcal{R}} = 0$, the bounds reduce to zero, and global asymptotic stability is achieved.

Before proceeding with the controller design, the following lemmas are presented to support the subsequent stability analysis:

Lemma 1. *Consider the scalar differential inequality*[18]

$$\dot{V}(t) \leq -\gamma V(t) + \delta \tag{8}$$

with $\gamma > 0$ and $\delta \geq 0$. Then, for all $t \geq 0$

$$V(t) \leq \exp^{-\gamma t} V(0) + \frac{\delta}{\gamma} \tag{9}$$

Lemma 2. *If there exists a continuously differentiable positive definite function $V(t)$ and positive constants c_1, c_2, γ, δ such that $c_1 \| \mathbf{x} \|^2 \leq V(t) \leq c_2 \| \mathbf{x} \|^2$ and $\dot{V}(t) \leq -\gamma \| \mathbf{x} \|^2 + \delta$ for all $t \geq 0$, then the system is uniformly ultimately bounded (UUB) and the solution satisfies*[18]

$$\| \mathbf{x}(t) \| \leq \sqrt{\frac{c_2}{c_1}} \| \mathbf{x}(0) \| \exp^{-\frac{\gamma}{2c_2}t} + \sqrt{\frac{\delta}{c_1\gamma}}, \quad \forall t \geq 0 \tag{10}$$

Lemma 3. *[Young's inequality]*[19] *For any vectors $\mathbf{a}, \mathbf{b} \in \mathbb{R}^n$ and a scalar $\eta > 0$,*

$$\mathbf{a}^T\mathbf{b} \leq \eta \| \mathbf{a} \|^2 + \frac{1}{4\eta} \| \mathbf{b} \|^2 \tag{11}$$

3. PROPOSED CONTROL METHODOLOGY

Motivated by the SLC framework developed in[13–15], the proposed control law combines PD control with the reuse of prior control information as a compact memory mechanism. This design accelerates transient convergence while maintaining robustness against bounded disturbances. The general formulation of the proposed composite PD-SLC law is expressed as

$$\mathcal{U}_\ell(t) = k_1 \underbrace{\mathcal{U}_\ell(t-\tau)}_{\text{learning term}} + \underbrace{(1-k_1)\,\mathcal{U}_{pd,\ell}(t)}_{\text{updating term}}, \quad \ell \in \{\mathcal{P}, \mathcal{R}\} \tag{12}$$

where $k_1 \in (0, 1)$ is the *learning intensity* controlling the weight assigned to prior control information, and $\tau > 0$ is the *learning interval*. The learning term $k_1\,\mathcal{U}_\ell(t-\tau)$ carries forward the control effort from the previous interval, while the updating term $(1-k_1)\,\mathcal{U}_{pd,\ell}(t)$ injects a fresh correction driven by the current tracking error. The weighting factor $(1-k_1)$ of the updating term ensures that the steady-state gain remains unity, preventing any static tracking offset.

In the following subsections, the general control framework (12) is applied to the position and attitude subsystems, as illustrated in Figure 1.

3.1. Position Control Subsystem. The position subsystem governs the translational motion of the quadrotor in 3D

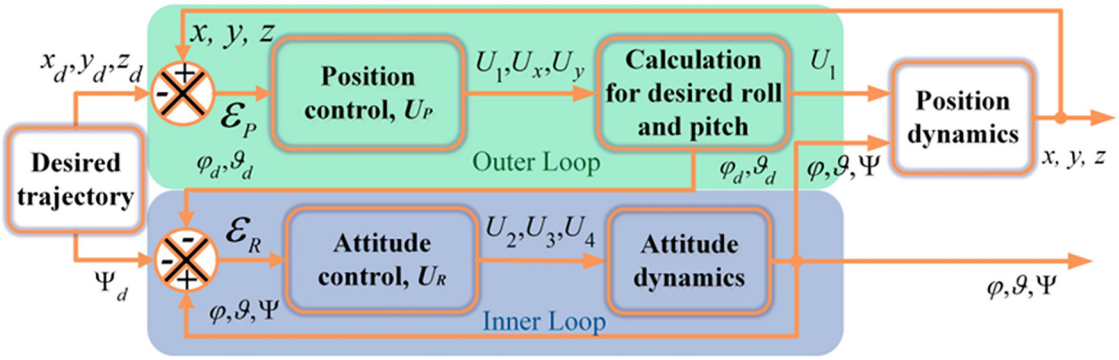

Figure 1. Schematic diagram of the closed-loop control implementation of trajectory tracking for UAVs

space. The PD updating term for the position subsystem is constructed as

$$\mathcal{U}_{pd,\mathcal{P}}(t) = \ddot{P}_d + \mathcal{K}_{p,\mathcal{P}}\,\delta_{\mathcal{P}1} + \mathcal{K}_{d,\mathcal{P}}\,\delta_{\mathcal{P}2} \in \mathbb{R}^3 \tag{13}$$

where $\mathcal{K}_{p,\mathcal{P}} = \mathrm{diag}\left(K_{p,z}, K_{p,x}, K_{p,y}\right) \succ 0$ and $\mathcal{K}_{d,\mathcal{P}} = \mathrm{diag}\left(K_{d,z}, K_{d,x}, K_{d,y}\right) \succ 0$ are the proportional and derivative gain matrices, respectively. Applying the general PD-SLC framework (12), the self-learning position control law is as follows:

$$\begin{aligned}\mathcal{U}_{\mathcal{P}}(t) &= k_1\,\mathcal{U}_{\mathcal{P}}(t-\tau)\\ &\quad + (1-k_1)\left(\ddot{P}_d + \mathcal{K}_{p,\mathcal{P}}\,\delta_{\mathcal{P}1} + \mathcal{K}_{d,\mathcal{P}}\,\delta_{\mathcal{P}2}\right)\end{aligned} \tag{14}$$

where $\mathcal{U}_{\mathcal{P}}(t) = [\mathrm{a}_z(t), \mathrm{a}_x(t), \mathrm{a}_y(t)]^T \in \mathbb{R}^3$ is the virtual acceleration vector.

From the position dynamics (2), the total thrust is computed from the altitude component as

$$U_1 = \frac{m}{\cos\varphi\,\cos\vartheta}\left(g + \mathrm{a}_z(t)\right) \tag{15}$$

The desired roll and pitch angles are extracted from the horizontal acceleration components $\mathrm{a}_x(t)$ and $\mathrm{a}_y(t)$ using the decoupled inverse kinematic relationship:

$$\varphi_d = \arcsin\left(\mathrm{sat}\left(\frac{\alpha_x \sin\Psi - \alpha_y \cos\Psi}{g}, \overleftarrow{\varphi}\right)\right) \tag{16}$$

$$\vartheta_d = \arcsin\left(\mathrm{sat}\left(\frac{\alpha_x \cos\Psi + \alpha_y \sin\Psi}{g\cos\varphi_d}, \overleftarrow{\vartheta}\right)\right) \tag{17}$$

where $\overleftarrow{\varphi}$ and $\overleftarrow{\vartheta}$ are the maximum allowable tilt angles and $\mathrm{sat}\left(\cdot, \overleftarrow{v}\right) = \mathrm{sign}(\cdot)\min(|\cdot|, \overleftarrow{v})$ is the saturation function. The time derivatives $\dot{\varphi}_d$, $\ddot{\varphi}_d$, $\dot{\vartheta}_d$, and $\ddot{\vartheta}_d$, required by the attitude subsystem, are obtained through the low pass filtered numerical differentiator:

$$\dot{\varphi}_d(t) = \alpha\,\dot{\varphi}_d(t-\Delta t) + (1-\alpha)\,\frac{\varphi_d(t) - \varphi_d(t-\Delta t)}{\Delta t} \tag{18}$$

where $\alpha \in (0,1)$ is the filter coefficient and Δt is the sampling period. The same filter structure is applied to obtain $\dot{\vartheta}_d$ and the corresponding second derivatives.

3.2. Attitude Control Subsystem. The attitude subsystem governs the rotational dynamics of the quadrotor. Defining the corresponding attitude tracking errors and their derivatives, we obtain

$$\begin{aligned} e_\varphi &= \varphi_d - \varphi, \dot{e}_\varphi = \dot{\varphi}_d - \dot{\varphi}\\ e_\vartheta &= \vartheta_d - \vartheta, \dot{e}_\vartheta = \dot{\vartheta}_d - \dot{\vartheta}\\ e_\Psi &= \Psi_d - \Psi, \quad \dot{e}_\Psi = \dot{\Psi}_d - \dot{\Psi}\end{aligned} \tag{19}$$

Note that the scalar errors e_φ, e_ϑ, ande_Ψ defined here correspond to the individual components of the vector error $\delta_{R1} = E_R$ used in the error dynamics (5). Furthermore, *U1* denotes the physical thrust input computed in (15), while U_x and U_y are virtual acceleration inputs forming the vector $U_p = [U_1, U_x, U_y]^{\mathrm{T}}$ in (14).

The PD updating term for the attitude subsystem is given as

$$\mathcal{U}_{pd,\mathcal{R}}(t) = \begin{bmatrix} \frac{\mathcal{J}_x}{l}\left(\ddot{\varphi}_d + K_{p,\varphi}\,e_\varphi + K_{d,\varphi}\dot{e}_\varphi\right)\\ \frac{\mathcal{J}_y}{l}\left(\ddot{\vartheta}_d + K_{p,\vartheta}\,e_\vartheta + K_{d,\vartheta}\dot{e}_\vartheta\right)\\ \mathcal{J}_z\left(\ddot{\Psi}_d + K_{p,\Psi}e_\Psi + K_{d,\Psi}\dot{e}_\Psi\right)\end{bmatrix} \in \mathbb{R}^3 \tag{20}$$

where $K_{p,(\cdot)} > 0$ and $K_{d,(\cdot)} > 0$ are the proportional and derivative gains for the corresponding rotational axis, and l is the arm length. Applying the general PD-SLC framework (12), the self-learning attitude control law is

$$\mathcal{U}_{\mathcal{R}}(t) = k_1\,\mathcal{U}_{\mathcal{R}}(t-\tau) + (1-k_1)\,\mathcal{U}_{pd,\mathcal{R}}(t) \tag{21}$$

where $\mathcal{U}_{\mathcal{R}}(t) = [U_2(t), U_3(t), U_4(t)]^T \in \mathbb{R}^3$ is the attitude control input vector.

Remark 1. *The full control input of the quadrotor is* $\mathcal{U}(t) = [U_1(t), U_2(t), U_3(t), U_4(t)]^T \in \mathbb{R}^4$, *where* U_1 *is computed from* (15) *and* $[U_2, U_3, U_4]^T$ *from* (21). *The controllers are subject to the actuator saturation constraint* $\| \mathcal{U}(t) \|_\infty \leq \mathcal{U}_{\max}$, *where* $\mathcal{U}_{\max} = [U_{1,\max}, U_{2,\max}, U_{3,\max}, U_{4,\max}]^T \in \mathbb{R}^4$ *is the maximum actuation limit.*

3.3. Stability Analysis. Because the position and attitude controllers share the same PD-SLC structure (12), the stability proof for both subsystems is carried out in a unified manner with an index $\ell \in \{\mathcal{P}, \mathcal{R}\}$. The *learning difference* in the control input is defined as [13]

$$\tilde{\mathcal{U}}_\ell(t) := \mathcal{U}_\ell(t) - \mathcal{U}_\ell(t-\tau) \tag{22}$$

Since the actuator outputs are bounded and the control signal evolves continuously, $\| \mathcal{U}_\ell(t) \|$ with $\alpha_\tau \to 0$ as $\tau \to 0$ [13,15].

Equivalent Algebraic Form

To avoid infinite recursion when handling the delayed control $\mathcal{U}_\ell(t-\tau)$ in the stability analysis, we note that $\mathcal{U}_\ell(t-\tau) = \mathcal{U}_\ell(t) - \dot{\tilde{\mathcal{U}}}_\ell(t)$. Substituting $\mathcal{U}_\ell(t) = k_1\mathcal{U}_\ell(t-\tau) + (1-k_1)\mathcal{U}_{pd,\ell}(t)$ from (12) and solving for $\mathcal{U}_\ell(t)$ yields the equivalent algebraic form[15]:

$$\mathcal{U}_\ell(t) = \underbrace{\mathcal{U}_{pd,\ell}(t)}_{\text{PD+feedforward}} - \underbrace{\kappa_2\tilde{\mathcal{U}}_\ell(t)}_{\text{learning residual}} \tag{23}$$

where

$$\kappa_2 := \frac{k_1}{1-k_1} \tag{24}$$

Thus, the PD-SLC law is equivalent to the nominal PD controller with feedforward, perturbed by the learning residual $\kappa_2\tilde{\mathcal{U}}_\ell(t)$, which vanishes as $\tau \to 0$. Consequently, the delayed control input can be expressed as

$$\mathcal{U}_\ell(t-\tau) = \mathcal{U}_\ell(t) - \tilde{\mathcal{U}}_\ell(t) = \mathcal{U}_{pd,\ell}(t) - (\kappa_2+1)\,\tilde{\mathcal{U}}_\ell(t) \tag{25}$$

Closed-Loop Error Dynamics

Recalling the error dynamics from (6) and (5), for each subsystem ℓ, the second-order error dynamics can be written as

$$\ddot{\boldsymbol{\delta}}_{\ell 1} = \mathcal{F}_\ell + \mathcal{G}_\ell\mathcal{U}_\ell(t) + \mathcal{D}_\ell - \ddot{\mathcal{S}}_{\ell,d} \tag{26}$$

where $\ddot{\mathcal{S}}_{\mathcal{P},d} = \ddot{\mathcal{P}}_d$ and $\ddot{\mathcal{S}}_{\mathcal{R},d} = \ddot{\mathcal{R}}_d$. Now, substituting the raw SLC law (12) directly into (26) yields

$$\begin{aligned}\ddot{\boldsymbol{\delta}}_{\ell 1} &= \mathcal{F}_\ell + \mathcal{G}_\ell\left[k_1\mathcal{U}_\ell(t-\tau) + (1-k_1)\,\mathcal{U}_{pd,\ell}(t)\right] \\ &\quad + \mathcal{D}_\ell - \ddot{\mathcal{S}}_{\ell,d} \\ &= \mathcal{F}_\ell + (1-k_1)\,\mathcal{G}_\ell\left(\ddot{\mathcal{S}}_{\ell,d} + \mathcal{K}_{p,\ell}\,\boldsymbol{\delta}_{\ell 1} + \mathcal{K}_{d,\ell}\,\boldsymbol{\delta}_{\ell 2}\right) \\ &\quad + k_1\,\mathcal{G}_\ell\,\mathcal{U}_\ell(t-\tau) + \mathcal{D}_\ell - \ddot{\mathcal{S}}_{\ell,d}\end{aligned} \tag{27}$$

Defining the augmented error state $\boldsymbol{\xi}_\ell = [\boldsymbol{\delta}_{\ell 1}^T,\ \boldsymbol{\delta}_{\ell 2}^T]^T \in \mathbb{R}^6$ and collecting terms, the closed-loop error dynamics take the following form:

$$\dot{\boldsymbol{\xi}}_\ell = \Phi_\ell\,\boldsymbol{\xi}_\ell + \Psi_\ell\,\mathcal{U}_\ell(t-\tau) + \mathbf{B}_\ell\,\mathbf{w}_\ell(t) \tag{28}$$

where

$$\Phi_\ell := \begin{bmatrix} 0_{3\times3} & \mathbf{I}_{3\times3} \\ (1-k_1)\,\mathcal{G}_\ell\,\mathcal{K}_{p,\ell} & (1-k_1)\,\mathcal{G}_\ell\,\mathcal{K}_{d,\ell}\end{bmatrix} \in \mathbb{R}^{6\times6} \tag{29}$$

$$\Psi_\ell := k_1\begin{bmatrix} 0_{3\times3} \\ \mathcal{G}_\ell\end{bmatrix} \in \mathbb{R}^{6\times3} \tag{30}$$

$$\mathbf{B}_\ell := \begin{bmatrix} 0_{3\times3} \\ \mathbf{I}_{3\times3}\end{bmatrix} \in \mathbb{R}^{6\times3} \tag{31}$$

and the lumped perturbation is

$$\mathbf{w}_\ell(t) := \mathcal{F}_\ell + \mathcal{D}_\ell - k_1\,\ddot{\mathcal{S}}_{\ell,d} \in \mathbb{R}^3 \tag{32}$$

Since the disturbances are bounded (Assumption 1), the nonlinear coupling $\mathcal{F}_\ell$ is bounded for bounded states. If the desired trajectory is smooth and bounded, there exists a constant $\overleftarrow{w}_\ell > 0$ such that $\|\,\mathbf{w}_\ell(t)\,\| \le \overleftarrow{w}_\ell$ for all $t \ge 0$.

Remark 2. *The dynamics (28) separate the nominal closed-loop behavior (through Φ_ℓ) from the learning coupling (through Ψ_ℓ). The matrix Φ_ℓ captures the PD error feedback scaled by $(1-k_1)$, while Ψ_ℓ carries the influence of the delayed control signal scaled by the learning intensity k_1. This structure parallels the self-learning consensus dynamics in*[15]*, adapted here for single-UAV trajectory tracking with nonlinear dynamics.*

Theorem 1. *Consider the error dynamics (6)−(5) for each subsystem $\ell \in \{\mathcal{P}, \mathcal{R}\}$ subject to Assumption 1. Under the proposed PD-SLC law (12) with $k_1 \in (0,1)$ and sufficiently small learning interval $\tau > 0$, if the gain matrices $\mathcal{K}_{p,\ell} \succ 0$ and $\mathcal{K}_{d,\ell} \succ 0$ are chosen such that there exist symmetric positive definite matrices $P_\ell = P_\ell^T \succ 0$ and $Q_\ell = Q_\ell^T \succ 0$ satisfying the matrix inequality*

$$\Xi_\ell := \frac{1}{2}\left(P_\ell\,\Phi_\ell + \Phi_\ell^T P_\ell\right) + Q_\ell + \frac{\kappa_1}{2}\left(P_\ell\,\Psi_\ell + \Psi_\ell^T P_\ell\right) \prec 0 \tag{33}$$

where $\kappa_1 := k_2/(1-k_1)$ with $k_2 = (1-k_1)$ denoting the updating weight so that $\kappa_1 = 1$, then the error $\boldsymbol{\xi}_\ell(t)$ is UUB and satisfies

$$\limsup_{t\to\infty} \|\,\boldsymbol{\xi}_\ell(t)\,\| \le \sqrt{\frac{2\,\delta_\ell}{\lambda_\ell^\star\,\lambda_{\min}(P_\ell)}} =: b_\ell \tag{34}$$

where $\lambda_\ell^\star > 0$ and $\delta_\ell \ge 0$ are defined in (44) and (45), respectively.

Proof: Consider the Lyapunov-Krasovskii functional[15]

$$V_\ell(t) = \frac{1}{2}\,\boldsymbol{\xi}_\ell^T(t)\,P_\ell\,\boldsymbol{\xi}_\ell(t) + \int_{t-\tau}^{t} \boldsymbol{\xi}_\ell^T(\zeta)\,Q_\ell\,\boldsymbol{\xi}_\ell(\zeta)\,d\zeta \tag{35}$$

where $P_\ell = P_\ell^T \succ 0$ and $Q_\ell = Q_\ell^T \succ 0$. Differentiating along the closed-loop trajectories (28) yields

$$\begin{aligned}\dot{V}_\ell(t) &= \boldsymbol{\xi}_\ell^T P_\ell\,\dot{\boldsymbol{\xi}}_\ell + \boldsymbol{\xi}_\ell^T Q_\ell\,\boldsymbol{\xi}_\ell - \boldsymbol{\xi}_{\ell,\tau}^T Q_\ell\,\boldsymbol{\xi}_{\ell,\tau} \\ &= \boldsymbol{\xi}_\ell^T P_\ell\left(\Phi_\ell\,\boldsymbol{\xi}_\ell + \Psi_\ell\,\mathcal{U}_\ell(t-\tau) + \mathbf{B}_\ell\,\mathbf{w}_\ell\right) \\ &\quad + \boldsymbol{\xi}_\ell^T Q_\ell\,\boldsymbol{\xi}_\ell - \boldsymbol{\xi}_{\ell,\tau}^T Q_\ell\,\boldsymbol{\xi}_{\ell,\tau}\end{aligned} \tag{36}$$

where $\boldsymbol{\xi}_{\ell,\tau} := \boldsymbol{\xi}_\ell(t-\tau)$. To handle the delayed control term $\mathcal{U}_\ell(t-\tau)$ without infinite recursion, we substitute the equivalent algebraic form (25):

$$\mathcal{U}_\ell(t-\tau) = \mathcal{U}_{pd,\ell}(t) - (\kappa_2+1)\,\tilde{\mathcal{U}}_\ell(t) \tag{37}$$

Since $\mathcal{U}_{pd,\ell}(t) = \ddot{\mathcal{S}}_{\ell,d} + \mathcal{K}_{p,\ell}\,\boldsymbol{\delta}_{\ell 1} + \mathcal{K}_{d,\ell}\,\boldsymbol{\delta}_{\ell 2}$, the term $\Psi_\ell\,\mathcal{U}_{pd,\ell}$ contains a component linear in $\boldsymbol{\xi}_\ell$ and a bounded feedforward term. Defining $\kappa_1 := 1$ (since the updating weight is $(1-k_1)$ and $\kappa_1 = (1-k_1)/(1-k_1) = 1$), then

$$\begin{aligned}\boldsymbol{\xi}_\ell^T P_\ell\,\Psi_\ell\,\mathcal{U}_\ell(t-\tau) &= \kappa_1\,\boldsymbol{\xi}_\ell^T P_\ell\,\Psi_\ell\,\boldsymbol{\xi}_{\ell'} + \boldsymbol{\xi}_\ell^T P_\ell\,\Psi_\ell\,\ddot{\mathcal{S}}_{\ell,d} \\ &\quad - (\kappa_2+1)\,\boldsymbol{\xi}_\ell^T P_\ell\,\Psi_\ell\,\tilde{\mathcal{U}}_\ell\end{aligned} \tag{38}$$

where $\boldsymbol{\xi}_{\ell'}$ collects the PD gain terms from $\mathcal{U}_{pd,\ell}$. Absorbing the bounded feedforward into $\mathbf{w}_\ell$ and noting $-\boldsymbol{\xi}_{\ell,\tau}^T Q_\ell\,\boldsymbol{\xi}_{\ell,\tau} \le 0$, Eq. (36) becomes

$$\begin{aligned}\dot{V}_\ell(t) &\le \boldsymbol{\xi}_\ell^T\left(P_\ell\,\Phi_\ell + Q_\ell + \kappa_1\,P_\ell\,\Psi_\ell\right)\boldsymbol{\xi}_\ell \\ &\quad -\boldsymbol{\xi}_\ell^T P_\ell\,\Psi_\ell\,(\kappa_2+1)\,\tilde{\mathcal{U}}_\ell + \boldsymbol{\xi}_\ell^T P_\ell\,\mathbf{B}_\ell\,\mathbf{w}_\ell\end{aligned} \tag{39}$$

Since (33) holds, taking the symmetric part of the quadratic form, there exists $\lambda_\ell > 0$ such that

$$\boldsymbol{\xi}_\ell^T\left(P_\ell\,\Phi_\ell + Q_\ell + \kappa_1\,P_\ell\,\Psi_\ell\right)\boldsymbol{\xi}_\ell \le -\lambda_\ell\ \|\,\boldsymbol{\xi}_\ell\,\|^2 \tag{40}$$

The remaining cross terms in (39) are bounded using Young's inequality (Lemma 3) with parameters $\eta_1, \eta_2 > 0$:

$$-\boldsymbol{\xi}_\ell^T P_\ell \Psi_\ell (\kappa_2+1)\tilde{\mathcal{U}}_\ell \leq \eta_1 \| \boldsymbol{\xi}_\ell \|^2 + \frac{(\kappa_2+1)^2}{4\eta_1} \| P_\ell \Psi_\ell \|^2 \alpha_\tau^2 \quad (41)$$

$$\boldsymbol{\xi}_\ell^T P_\ell \mathbf{B}_\ell \mathbf{w}_\ell \leq \eta_2 \| \boldsymbol{\xi}_\ell \|^2 + \frac{1}{4\eta_2} \| P_\ell \mathbf{B}_\ell \|^2 \overleftarrow{w}_\ell^2 \quad (42)$$

Substituting (40)–(42) into (39) and choosing η_1, η_2 small enough so that $\lambda_\ell^\star := \lambda_\ell - \eta_1 - \eta_2 > 0$,

$$\dot{V}_\ell(t) \leq -\lambda_\ell^\star \| \boldsymbol{\xi}_\ell \|^2 + \delta_\ell \quad (43)$$

where

$$\lambda_\ell^\star := \lambda_\ell - \eta_1 - \eta_2 > 0 \quad (44)$$

$$\delta_\ell := \frac{(\kappa_2+1)^2}{4\eta_1} \| P_\ell \Psi_\ell \|^2 \alpha_\tau^2 + \frac{1}{4\eta_2} \| P_\ell \mathbf{B}_\ell \|^2 \overleftarrow{w}_\ell^2 \quad (45)$$

Since $V_\ell(t) \geq \frac{1}{2}\lambda_{\min}(P_\ell) \| \boldsymbol{\xi}_\ell \|^2$, Inequality (43) gives

$$\dot{V}_\ell(t) \leq -\frac{2\lambda_\ell^\star}{\lambda_{\max}(P_\ell)} V_\ell(t) + \delta_\ell \quad (46)$$

Applying Lemma 1 to (46) with $\gamma = 2\lambda_\ell^\star / \lambda_{\max}(P_\ell)$,

$$V_\ell(t) \leq \exp\left(-\frac{2\lambda_\ell^\star}{\lambda_{\max}(P_\ell)} t\right) V_\ell(0) + \frac{\delta_\ell \lambda_{\max}(P_\ell)}{2\lambda_\ell^\star} \quad (47)$$

It follows from Lemma 2 with $c_1 = \frac{1}{2}\lambda_{\min}(P_\ell)$, $c_2 = \frac{1}{2}\lambda_{\max}(P_\ell) + \tau \lambda_{\max}(Q_\ell)$, $\gamma = \lambda_\ell^\star$, and $\delta = \delta_\ell$ that $\boldsymbol{\xi}_\ell(t)$ is UUB and converges exponentially to the residual set $\mathcal{B}_\ell = \{\boldsymbol{\xi}_\ell : \| \boldsymbol{\xi}_\ell \| \leq b_\ell\}$ with

$$b_\ell = \sqrt{\frac{2\delta_\ell}{\lambda_\ell^\star \lambda_{\min}(P_\ell)}} \quad (48)$$

which establishes (34) and completes the proof.

Remark 3. *The ultimate bound b_ℓ in (48) depends on δ_ℓ in (45), which contains two contributions: (i) the learning residual term scaled by α_τ^2, and (ii) the lumped perturbation term scaled by $\overleftarrow{w}_\ell^2$. Since $\alpha_\tau \to 0$ as $\tau \to 0$ [13,15], reducing the learning interval directly tightens b_ℓ, and the scheme approaches the ideal PD tracking performance. In the disturbance-free case, i.e., when $\mathcal{D}_\ell = 0, \mathcal{F}_\ell = 0$, and $\tau \to 0$, both $\overleftarrow{w}_\ell$ and α_τ vanish, the bound reduces to zero, and global asymptotic stability is recovered. Selecting τ as one or a few sampling periods is recommended in practice [15].*

Remark 4. *The matrix inequality (33) is satisfied by choosing the PD gains large enough to dominate the nonlinear coupling $\mathcal{F}_\ell$ and $k_1 \in (0,1)$ to keep κ_2 finite. Since Φ_ℓ in (29) has the structure of a second-order linear system with positive definite gain matrices, any positive definite choice of $\mathcal{K}_{p,\ell}$ and $\mathcal{K}_{d,\ell}$ ensures the existence of $P_\ell \succ 0$ satisfying (33). The practical tuning sequence follows directly: fix τ first according to hardware constraints, select the PD gains for baseline stability, then increase k_1 to accelerate convergence [15].*

To further verify the stability condition associated with the proposed gain selection, a root-locus analysis was conducted, as presented in Figure 2. It can be observed that, for the chosen positive controller gains, all system eigenvalues remain in the left half of the *s*-plane, confirming the asymptotic stability of the closed-loop system. Moreover, the eigenvalue trajectories illustrate that the proposed gain variations preserve system stability while improving transient response characteristics. This analysis provides additional justification for the matrix condition employed in the stability proof.

4. SIMULATION RESULTS

The performance of the proposed PD-SLC scheme was evaluated through numerical simulations in MATLAB/Simulink. The physical parameters of the quadrotor were set as follows: mass $m = 0.65$ kg, gravitational acceleration $g = 9.81$ m/s^2, arm length $l = 0.23$ m, and moments of inertia $J_x = J_y = 7.5 \times 10^{-3}$ N·m·s^2/rad and $J_z = 1.3 \times 10^{-2}$ N·m·s^2/rad. To assess robustness, the quadrotor was subjected to time-varying external disturbances, modeled as $\mathcal{D}_\mathcal{P} = [0.1\cos(0.1\pi t), 0.1\sin(0.1\pi t), 0.1\cos(0.1\pi t)]^\mathrm{T}$ and $\mathcal{D}_\mathcal{R} = [0.1\sin(0.1\pi t), 0.1\cos(0.1\pi t), 0.1\sin(0.1\pi t)]^\mathrm{T}$. Sinusoidal disturbances were selected to emulate realistic time-varying aerodynamic effects commonly encountered in UAV applications, such as wind gusts and oscillatory airflow. The PD-SLC parameters were set to $k_1 = 0.85$, $\tau = 0.01$ s, $\alpha = 0.85$, and sampling period $\Delta t = 0.001$ s. The outer-loop gains were $K_{p,x} = K_{p,y} = 1.5$ and $K_{d,x} = K_{d,y} = 1.6$, while the inner-loop gains were $K_{p,z} = 4.0$, $K_{d,z} = 2.5$, $K_{p,\phi} = K_{p,\theta} = 3.0$, $K_{d,\phi} = K_{d,\theta} = 1.5$, $K_{p,\psi} = 2.0$, and $K_{d,\psi} = 1.0$. To demonstrate effectiveness, the proposed scheme was compared against two well-established benchmark controllers: conventional SMC and PID control. For SMC, a linear sliding surface was employed, with proportional and switching gains set to $k_p = 2$ and $k_s = 0.5$, respectively. For PID, the gain matrices were chosen as $Kp = \mathrm{diag}(3,3,4)$, $Kd = \mathrm{diag}(3,3,2.5)$, and $Ki = \mathrm{diag}(0.5,0.5,0.5)$. These control parameters were tuned to ensure stable and fair comparative performance under varying operating conditions. Finally, two case studies were conducted using different reference trajectories.

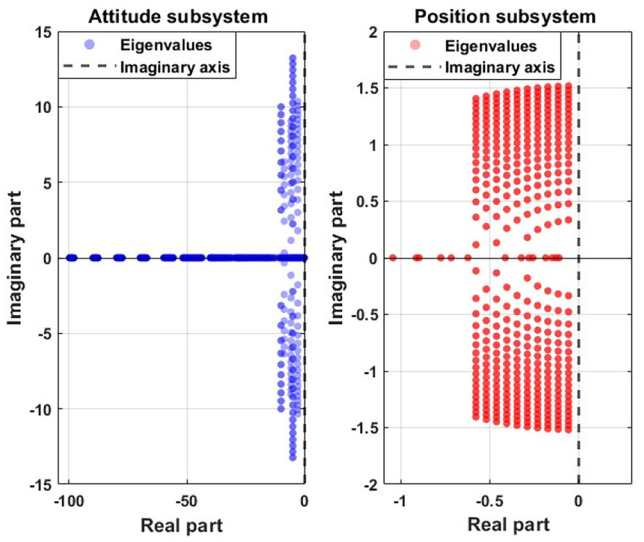

Figure 2. Root locus of the two subsystems with respect to proportional gain

Case 1: Helical Trajectory Tracking

In this case, a helical trajectory is adopted, defined as $z_d = t/10$, $x_d = 2\sin(2\pi t/40)$, $y_d = \sin(4\pi t/40)$, and $\psi_d = 0.0872\sin(2\pi t/40)$, with zero initial conditions. The 3D trajectory tracking and error responses under the different control schemes are presented in Figures 3 and 4, respectively. In the tracking response, despite initial deviations caused by the zero-start condition and external disturbances, the proposed PD-SLC successfully converges to the desired helical path within a short time, with its trajectory visually overlapping the reference earlier and more precisely than those of PID and SMC. Figure 4 illustrates the position and attitude error norms, i.e., $\| \mathcal{E}_{\mathcal{P}} \|$ and $\| \mathcal{E}_{\mathcal{R}} \|$, which converge to near-zero values within approximately 4 s under PD-SLC, outperforming PID and SMC in both transient speed and steady-state accuracy. The zoomed-in attitude error plot further reveals that the PID controller exhibits persistent low-amplitude oscillations of approximately 5×10^{-3} rad in steady state, which are absent under PD-SLC.

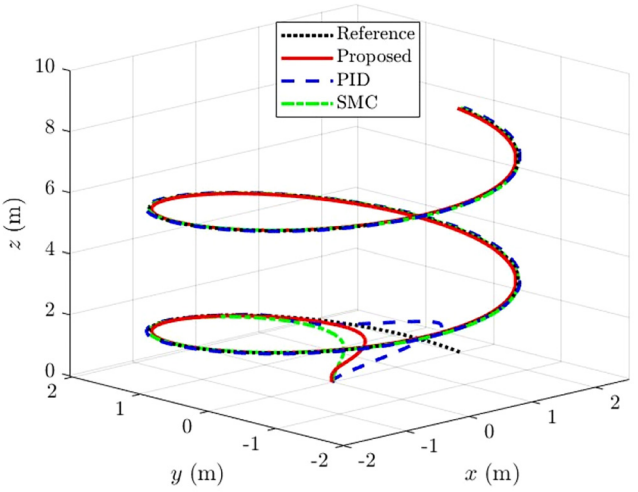

Figure 3. Helical-shaped three-dimensional trajectory tracking response

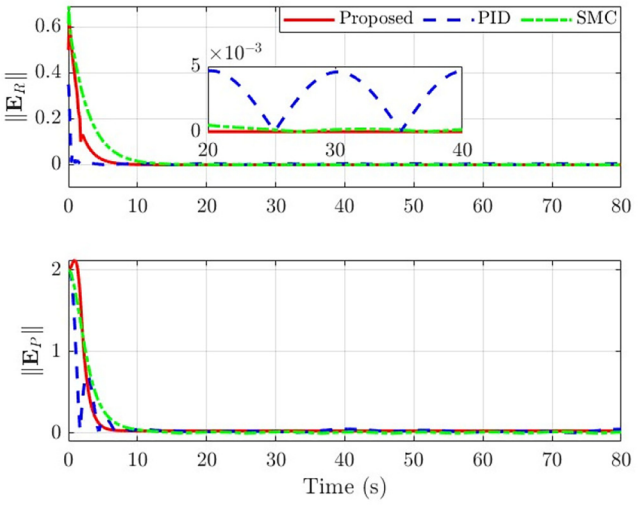

Figure 4. Attitude and position error norm responses during helical trajectory tracking under different control schemes

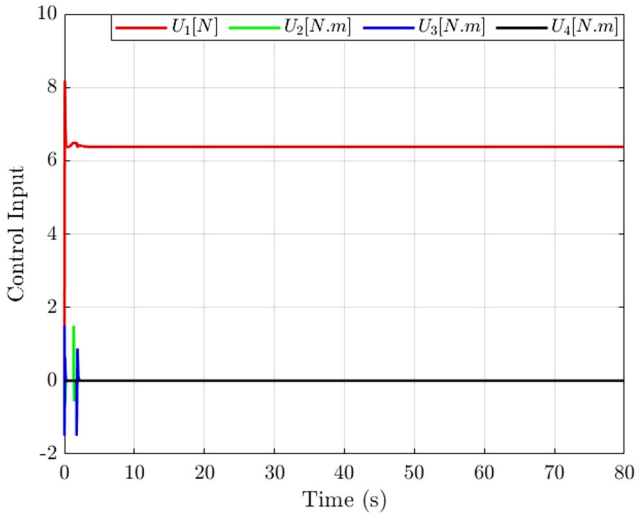

Figure 5. Control input response under helical trajectory

Table 1. *Error performance measures under helical trajectory tracking*

Approach	Performance indices				
	ISE	IAE	ITSE	ITAE	FCI
PID	6.2137	10.4252	8.4577	140.8192	510.9212
SMC	4.0673	7.2323	6.1127	77.7180	510.3402
Proposed PD-SLC	3.4344	5.4833	4.4164	60.3362	507.8205

The variation of the control inputs over time is shown in Figure 5. The thrust input U_1 quickly reaches the hover value of approximately 6.37 N, which is equal to mg, after a short transient around $t = 1$s. The torque inputs U_2, U_3, and U_4 exhibit small initial peaks and then rapidly settle close to zero. The proposed PD-SLC generates smooth and chatter-free control signals. This is achieved through the self-learning framework, which utilizes previous control inputs rather than relying on switching actions, resulting in smoother behavior. Such characteristics are crucial in real-world systems, as rapid fluctuations can damage actuators and induce undesirable vibrations.

Table 1 displays the error performance results for the different control methods. The proposed PD-SLC yields the lowest values across all performance indices, reducing the integral of squared error (ISE) by 44.7%, integral of absolute error (IAE) by 47.4%, integral of time-weighted squared error (ITSE) by 47.8%, and integral of time-weighted absolute error (ITAE) by 57.1% compared with PID. The SMC method achieves reductions of 15.6%, 24.2%, 27.8%, and 22.4% for the respective indices. Furthermore, the proposed method delivers superior tracking performance with reduced control effort, as reflected in lower fuel consumption index (FCI) values. Based on these findings, the self-learning approach is both efficient and effective.

Case 2: Lemniscate Trajectory Tracking

In this case study, a two-phase Lemniscate of Bernoulli trajectory is adopted. In the first phase, the quadrotor ascends vertically from rest while maintaining its horizontal position at the origin, following $z_d = h_c\, t/t_c$ for $0 \le t \le t_c$, where $h_c = 1$ m is the cruise altitude and $t_c = 10$ s is the climb duration.

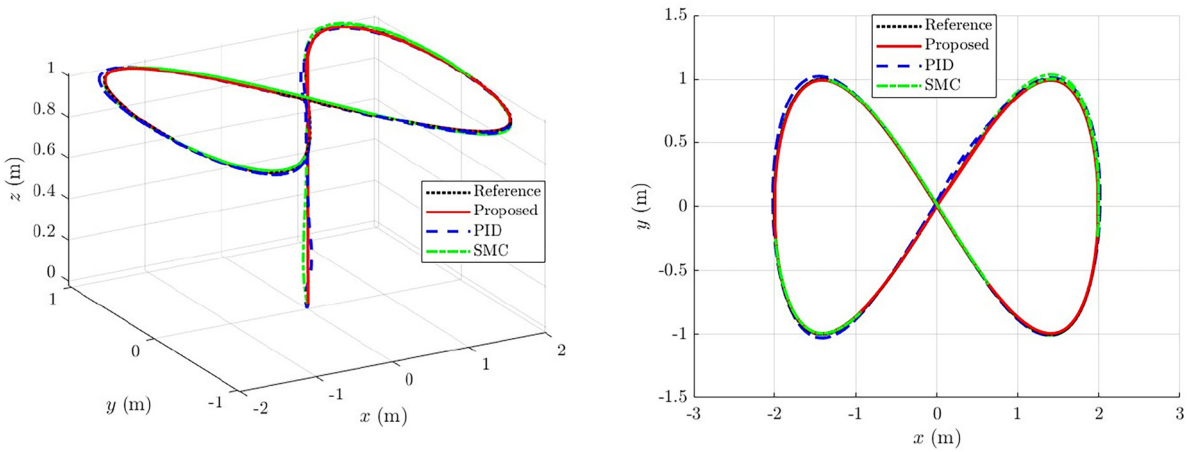

(a) Three-dimensional trajectory view (b) Two-dimensional plane projection

Figure 6. Lemniscate trajectory tracking responses under different control schemes

Once the cruise altitude is reached, the quadrotor transitions into the second phase and traces the lemniscate in the horizontal plane, defined by $x_d = a\sin(\omega t_s)$, $y_d = \frac{a}{2}\sin(2\omega t_s)$, $z_d = h_c$, and $\psi_d = \psi_0 \sin(\omega t_s)$. Here, $t_s = t - t_c$ is the shifted time from the start of the figure-eight phase, $a = 2$ m is the lemniscate scale, $\omega = 2\pi/60$ rad/s corresponds to one complete loop every 60 s, and $\psi_0 = 5°$. Because the trajectory repeatedly changes direction at the lobe-crossing points, Case 2 represents a more challenging scenario for evaluating transient performance compared with Case 1.

The 3D and 2D trajectory tracking responses are presented in Figure 6. In this case, the proposed PD-SLC closely follows the figure-eight reference across both lobes, handling the lobe-crossing maneuver smoothly without visible spikes or divergence. By contrast, the PID controller exhibits noticeable deviation near the crossing point where the velocity direction reverses, and the SMC shows moderate improvement but still lags behind the proposed method. These observations confirm that the self-learning memory term $k_1\mathbf{U}(t-\tau)$ acts as a stabilizing mechanism during rapid reference changes—an effect that neither PID nor SMC can replicate without additional complexity.

For this scenario, the attitude error $\| \mathcal{E}_{\mathcal{R}} \|$, shown in Figure 7, converges within approximately 2 s, while the position error $\| \mathcal{E}_{\mathcal{P}} \|$ settles to a significantly smaller residual bound compared with those of PID and SMC. The inset of the attitude error plot indicates that the PID controller exhibits persistent low-amplitude oscillations of about 5×10^{-3} rad during steady state, whereas such oscillations are absent in the proposed PD-SLC. Moreover, the position error responses of both PID and SMC display higher error spikes at lobe-crossing points, while the proposed PD-SLC effectively suppresses these spikes owing to the accumulated control memory.

The control inputs for Case 2 under the proposed scheme are shown in Figure 8. The thrust U_1 quickly settles around the hover value of approximately 6.4 N (equal to mg), whereas the torque inputs U_2, U_3, and U_4 remain close to zero once the UAV begins following the figure-eight trajectory. The proposed PD-SLC produces smooth, chatter-free control responses

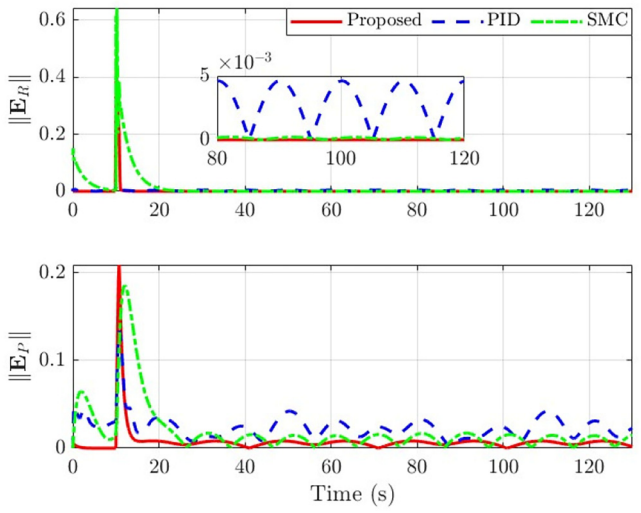

Figure 7. Attitude and position error norm responses during lemniscate trajectory tracking under different control schemes

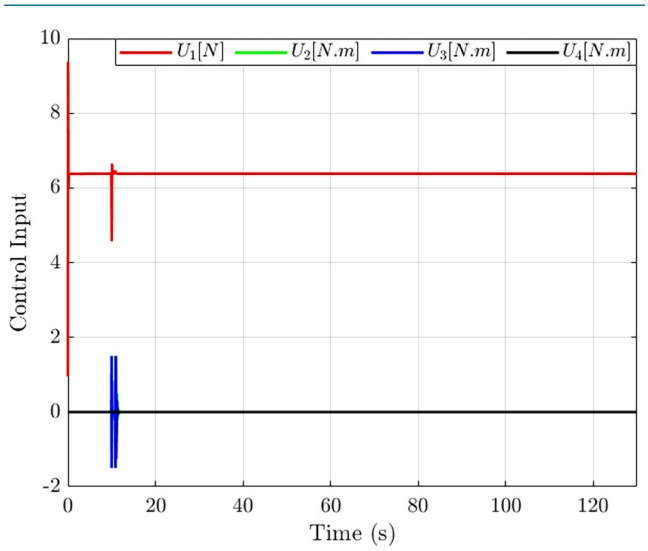

Figure 8. Control input under lemniscate trajectory

Table 2. *Error performance measures under lemniscate trajectory tracking*

Approach	Performance indices				
	ISE	IAE	ITSE	ITAE	FCI
PID	0.5260	2.5744	0.9384	61.7445	382.9411
SMC	0.2329	3.1984	0.6724	38.6494	382.6938
Proposed PD-SLC	0.1246	1.2499	0.1337	14.3923	379.6351

owing to its self-learning strategy (12). The quantitative error performance measures are listed in Table 2. The proposed method demonstrates significant improvements, with substantial reductions in ISE, IAE, ITSE, ITAE, and FCI compared with both PID and SMC. Specifically, PD-SLC achieves lower error indices and reduced control effort, highlighting the advantage of the self-learning mechanism. This capability is particularly beneficial under rapidly varying trajectories, where the use of historical control information enhances tracking performance without increasing control demand.

5. CONCLUSIONS

This paper presents a novel PD-SLC method for robust trajectory tracking of quadrotor systems under disturbances and uncertainties. The proposed approach leverages previous control input information to enhance system performance without requiring a complex design. Integration of the scheme with existing control techniques is straightforward, making it versatile for practical applications. By exploiting historical control data, the controller improves adaptability, achieves faster response, and reduces control effort. The stability of the closed-loop system was established using Lyapunov theory, ensuring that the tracking error remains bounded. Numerical simulations were conducted to evaluate the performance of the proposed method, and the results indicated improved tracking accuracy and robustness compared with conventional PID and SMC. Overall, the proposed scheme offers a simple yet effective solution for practical quadrotor control applications. Notably, the presented results are based on numerical simulations. Future work will focus on hardware-in-the-loop validation and experimental testing on a physical quadrotor platform to further confirm the practical effectiveness of the proposed scheme.

AFFILIATIONS AND AUTHOR DETAILS

Undergraduate Author

Abdulrahman Sulaiman Al-Sayed – *Control & Instrumentation Engineering Department, King Fahd University of Petroleum & Minerals (KFUPM), Dhahran 31261, Saudi Arabia*; 0009-0005-5766-366X
Email: s202251560@kfupm.edu.sa

Corresponding Author

Syed Muhammad Amrr – *Research Mentor, Assistant Professor, Control & Instrumentation Engineering Department & Interdisciplinary Research Center for Sustainable Energy Systems, King Fahd University of Petroleum & Minerals (KFUPM), Dhahran 31261, Saudi Arabia* 0000-0001-5084-5472
Email: syed.amrr@kfupm.edu.sa

ACKNOWLEDGEMENTS

The authors would like to thank Mr. Abdullah Abushokor, a Ph.D. student at CIE Department, KFUPM, for his valuable assistance in simulations, technical discussions, and valuable suggestions that contributed to the development of this work.

REFERENCES

(1) Abushokor, A., Amrr, S. M., Ferik, S. E. & Al-Dhaifallah, M. Optimized adaptive variable exponent nonsingular terminal SMC for trajectory tracking of a quadrotor. *J. Vib. Control,* **Early Access**, 10775463261422360 (2026).

(2) Mo, H. & Farid, G. Nonlinear and adaptive intelligent control techniques for quadrotor UAV—a survey. *Asian J. Control* **21 (2)**, 989–1008 (2019).

(3) Zuo, Z., Liu, C., Han, Q.-L. & Song, J. Unmanned aerial vehicles: Control methods and future challenges. *IEEE/CAA J. Autom. Sin.* **9 (4)**, 601–614 (2022).

(4) Wang, Q., Wang, W. & Suzuki, S. UAV trajectory tracking under wind disturbance based on novel antidisturbance sliding mode control. *Aerosp. Sci. Technol.* **149**, 109138 (2024).

(5) Abushokor, A. & Amrr, S. M. Variable exponent fixed-time optimized sliding mode for quadrotor attitude control. In *Proc. 60th IEEE Industry Applications Society Annual Meeting (IAS)*, 1–6 (2025).

(6) Moreno-Valenzuela, J., Pérez-Alcocer, R., Guerrero-Medina, M. & Dzul, A. Nonlinear PID-type controller for quadrotor trajectory tracking. *IEEE/ASME Trans. Mechatron.* **23 (5)**, 2436–2447 (2018).

(7) Amrr, S. M., Sarkar, R., Banerjee, A., Saidi, A. S. & un Nabi, M. Fault-tolerant finite-time adaptive higher order sliding mode control with optimized parameters for attitude stabilization of spacecraft. *Int. J. Robust Nonlinear Control* **32 (5)**, 2845–2863 (2022).

(8) Abushokor, A. & Amrr, S. M. Robust distributed formation tracking control for multi-UAVs under network constraint using event-triggered adaptive variable-exponent SMC. *IEEE J. Miniatur. Air Space Syst.* **7 (2)**, 246-259 (2026).

(9) Wang, B., Zhang, Y. & Zhang, W. A composite adaptive fault-tolerant attitude control for a quadrotor UAV with multiple uncertainties. *J. Syst. Sci. Complex.* **35**, 81–104 (2022).

(10) Mehmood, Y., Aslam, J., Ullah, N., Chowdhury, M. S., Techato, K. & Alzaed, A. N. Adaptive robust trajectory tracking control of multiple quad-rotor UAVs with parametric uncertainties and disturbances. *Sensors* **21**, 2401 (2021).

(11) Wang, J., Alattas, K. A., Bouteraa, Y., Mofid, O. & Mobayen, S. Adaptive finite-time backstepping control tracker for quadrotor UAV with model uncertainty and external disturbance. *Aerosp. Sci. Technol.* **133**, 108088 (2023).

(12) Mofid, O. & Mobayen, S. Adaptive finite-time backstepping global sliding mode tracker of quad-rotor UAVs under model uncertainty, wind perturbation, and input saturation. *IEEE Trans. Aerosp. Electron. Syst.* **58 (1)**, 140–151 (2022).

(13) Zhang, C., Xiao, B., Wu, J. & Li, B. On low-complexity control design to spacecraft attitude stabilization: An online-learning approach. *Aerosp. Sci. Technol.* **110**, 106441 (2021).

(14) Zhang, C., Ahn, C. K., Wu, J. & He, W. Online-learning control with weakened saturation response to attitude tracking: A variable learning intensity approach. *Aerosp. Sci. Technol.* **117**, 106981 (2021).

(15) Zhang, C. Self-learning control for multi-agent consensus. *Appl. Math.* **6 (3)**, 37 (2026).

(16) Zhang, C. Self-learning control under practical actuation. *Aerospace Engineering Communications* **1 (1)**, 36–46 (2026).

(17) Sabatino, F. *Quadrotor control: Modeling, nonlinear control design, and simulation*. Master's dissertation, KTH, Sweden (2015).

(18) Khalil, H. K. *Nonlinear systems*, 3rd ed. (Prentice Hall, 2002).

(19) Young, W. H. On classes of summable functions and their Fourier series. *Proc. R. Soc. Lond. A* **87**, 225–229 (1912).